An Algorithm for Calculating the Coupling Between MMICs with Block Dielectric Coverings

Zhaoyang Wang, *Student Member, IEEE,* and Robert W. Jackson, *Senior Member, IEEE*

***Abstract*—In this paper, a computer-aided design (CAD) algorithm is presented for determining the coupling between sealant covered monolithic microwave integrated circuits (MMICs) in a multichip module. It is assumed that the MMICs are sufficiently separated that near-field coupling can be neglected and that TM_0 parallel-plate fields dominate. It is also assumed that the MMICs are each covered by a sealant of size commensurate with the MMIC. The technique presented is computationally simple, appropriate for use with layout-based circuit CAD software, and uses no numerical electromagnetics. It has been tested by comparison to full-wave electromagnetic simulation. In simple test cases, this technique showed over two orders of magnitude increase in speed. For larger problems, the increase in speed will be more pronounced.**

***Index Terms*—Microwave multichip modules, microwave packaging model, MMIC CAD, MMIC coupling, MMIC sealant, module isolation.**

I. Introduction

TO ACHIEVE the goal of virtual prototyping of microwave (MW) and millimeter-wave (MMW) designs, many capabilities must be dramatically improved in the current set of electronic design automation (EDA) tools. One of these capabilities is quick and accurate simulation of a completed MW/MMW multichip assembly (MCA). The computer-aided design (CAD) technique presented in this paper has been developed for calculating the coupling between the block dielectric covered monolithic microwave integrated circuits (MMICs) in an MCA. Coverings such as this occur when a sealant is applied for protection. As we will show, sealant coverings can increase the coupling between MMICs by tens of decibels.

Fig. 1 shows the basic configuration of a hypothetical MCA containing two MMICs embedded in substrate 1 and covered with a sealant of thickness d_s. The technique described in this paper extends the algorithm presented in [1]. In that paper, the middle layer in Fig. 1 was constrained to be homogeneous whereas, in this paper, the middle layer may contain sealant islands covering each MMIC. In principle, one could calculate the effect these islands have on MMIC-to-MMIC coupling by simulating the entire structure using a method of moments or, most likely, a finite-element simulator. For large complicated MMICs, this is impractical and unnecessary. Simplified numerical techniques have been developed for static or near-field coupling between dielectric covered MMICs [2], [3]. However, these techniques are still quite detailed and more sophisticated than necessary for the MCA problem. Furthermore, MMICs in an MCA are sufficiently separated that static or near-field coupling is usually negligible and only TM_0 full-wave fields are significant. This approximation (and others to be described) results in a new algorithm that uses computational resources roughly equivalent to a MW circuit simulator, but orders of magnitude less than is used by, for example, a finite-element simulator.

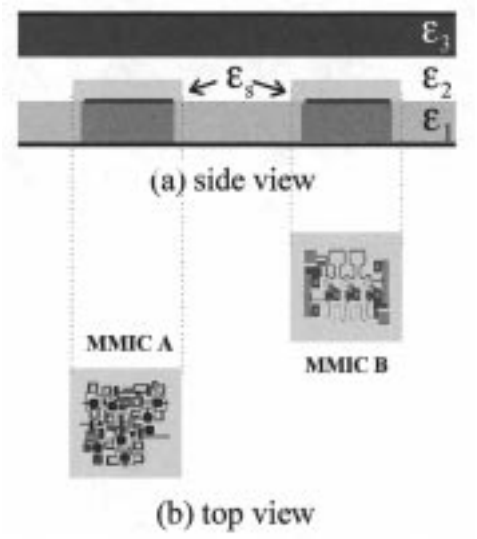

Fig. 1. Configuration of the MCA with block dielectric covered MMICs

In what follows, we describe in more detail the technique that was originally outlined in [4], and we present new material showing how the technique can be modified for use in a package with conducting walls. The basic idea, detailed in Section II, is to convert the inhomogeneous problem into an approximately equivalent homogeneous one—with no sealant islands. The resulting problem can then be solved using the equivalent dipole technique [1] and the procedure discussed in Section III. In Section IV, the algorithm is applied to a test case and the result compared to detailed full-wave simulation. The modification for laterally enclosed package is presented in Section V and verified by comparison to full-wave simulation in Section VI.

II. Inhomogeneous-to-Homogeneous Simplification

Using the technique described in [1], we can predict the coupling between two MMICs, i.e., A and B, by determining the voltages induced on the components that comprise MMIC B in response to the currents on the components that comprise

Manuscript received July 29, 1999. This work was supported by the Defense Advanced Research Projects Agency and by Raytheon under a Thrust 1 MAFET contract.

The authors are with the Department of Electrical and Computer Engineering, University of Massachusetts at Amherst, Amherst, MA 01003 USA (e-mail: zwang@ecs.umass.edu; jackson@ecs.umass.edu).

Publisher Item Identifier S 0018-9480(01)00027-8.

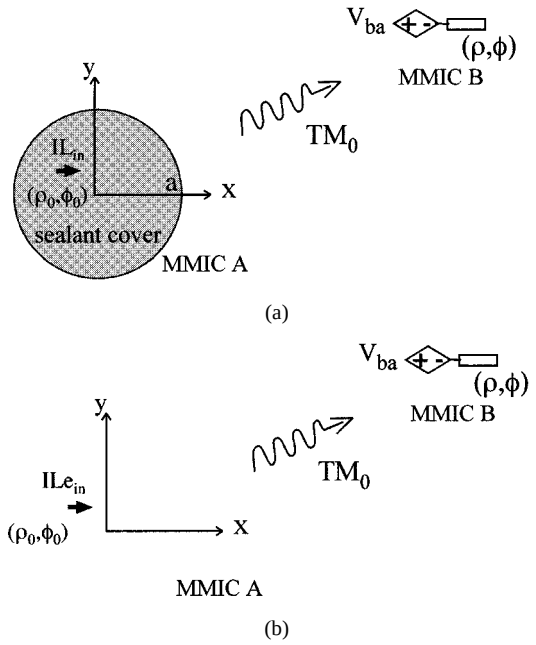

Fig. 2. Equivalent-current dipole produces the same voltage on MMIC B

MMIC A. Covering MMIC A with a dielectric block causes more energy to couple from it. Therefore, larger voltages are induced in MMIC B. To determine these larger voltages, an inhomogeneous problem needs to be solved. We can solve the inhomogeneous problem by finding an equivalent uncovered component that induces the same voltages as the dielectric covered component. After replacing all the dielectric block-covered components with their equivalent uncovered components, we reduce the inhomogeneous problem to a homogeneous one.

Fig. 2 shows the inhomogeneous-to-homogeneous simplification. Three assumptions are made in the problem. First, since MMICs A and B are widely separated, it is assumed that their coupling is due only to TM_0 parallel-plate waves. This implies that the conducting cover and ground plane are close enough to each other that all other parallel-plate waves are evanescent. Secondly, we assume for simplicity that the sealant cover is cylindrical. This is reasonable because sealant covers are usually shaped like a block with round corners or some other quasi-cylindrical shape. Thirdly, the sealant cover is assumed very thin in comparison to total thickness of the MCA. The third assumption allows the neglect of high-order modes excited at the edge of a sealant cover.

The detailed analysis using these simplifications is presented below.

A. Equivalent Factor for a Sealant Covered Dipole

The original inhomogeneous problem is illustrated in Fig. 2(a). As discussed in [1], a radiating component in MMIC A is approximated as an electrical dipole that has a moment $I_{\mathrm{in}}\vec{L}$ where

$$I_{\mathrm{in}}\vec{L} = \iint \vec{J}(x,\, y)\, dx\, dy \tag{1}$$

and $\vec{J}(x,\, y)$ is the current density on the component. I_{in} is the terminal current of the component and is calculated by a standard circuit simulator. $\vec{L}$ is the effective length of the component and represents the energy radiating performance of it. Using (1), $\vec{L}$ can be determined from the approximate shape of $\vec{J}$. For a wide range of components, $\vec{L}$ can be computed analytically and the results stored in a library.

When a dielectric block covers MMIC A, the radiating characteristics of each circuit element are changed by a factor we define as F. The adjusted effective length can be written as

$$\vec{L}e = F\vec{L}. \tag{2}$$

In Fig. 2(b), $I\vec{L}e$ is the equivalent electric dipole without a dielectric cover that produces the same voltage on a component in MMIC B as the original dipole $I\vec{L}$ in Fig. 2(a).

Since the factor F represents the change in the TM_0 wave at $(\rho,\, \phi)$ due to the effect of a sealant cover on an electric dipole, we can express F as

$$F = \Psi_c(\rho,\, \phi)/\Psi_a(\rho,\, \phi) \tag{3}$$

where ψ_c and ψ_a are the z-directed magnetic potentials of the TM_0 waves created by a dipole at $(\rho_0,\, \phi_0)$ with and without sealant cover.

A structure without sealant covers has three layers: a substrate, free-space layer, and top damping layer. We denote the TM_0 waves in the three-layer structure as TM_0^a waves. The magnetic potential Ψ_a of theTM_0^a waves created by an uncovered dipole at $(\rho_0,\, \phi_0)$ can be expressed as

$$\Psi_a = \sum_{n=-\infty}^{\infty} a_n^a H_n^{(2)}(\beta_0^a \rho) e^{jn\phi} f_a(z), \qquad \rho > \rho_0 \tag{4}$$

where β_0^a and $f_a(z)$ are the propagation constant and vertical distribution function of a TM_0^a mode. They can be determined in the usual manner by enforcing the boundary conditions at the interfaces of the three layers. The constants a_n^a depend on the location and orientation of the dipole under consideration. Expressions for them will be determined in Section II-B and II-C. We normalize $f_a(z)$ such that $f_a(0) = 1$.

When a sealant cover is in place, the structure in the region of $\rho < a$ has four layers [see Fig. 2(a)]. In that region, we denote the TM_0 waves in the four layers as TM_0^s waves. The propagation constant β_0^s and vertical distribution function $f_s(z)$ of a TM_0^s mode are then determined by the boundary condition at the interfaces of the four layers. We normalize $f_s(z)$ such that $f_s(0) = 1$. The structure outside the region with sealant cover still has only three layers. There, the TM_0 waves in three layers are TM_0^a waves.

The magnetic potentials of the TM_0 waves created by the sealant covered dipole at $(\rho_0,\, \phi_0)$ in the region $\rho > \rho_0$ can be expressed as

$$\Psi_c^- = \sum_{n=-\infty}^{\infty} a_n^c \left(H_n^{(2)}(\beta_0^s \rho) + R_n H_n^{(1)}(\beta_0^s \rho) \right) e^{jn\phi} f_s(z), \qquad a > \rho > \rho_0 \tag{5a}$$

$$\Psi_c^+ = \sum_{n=-\infty}^{\infty} a_n^c T_n H_n^{(2)}(\beta_0^a \rho) e^{jn\phi} f_a(z), \qquad \rho > a. \tag{5b}$$

Ψ_c^- consists of outward and inward traveling waves with radial dependence $H_n^{(2)}(\beta_0^s\rho)$ and $H_n^{(1)}(\beta_0^s\rho)$, respectively. R_n is the reflection coefficient of each TM_{0n}^s mode at the discontinuous boundary $\rho = a$. Ψ_c^+ consists of TM_0^a modes with radial dependence $H_n^{(2)}(\beta_0^a\rho)$. T_n is the transmission coefficient from TM_{0n}^s wave to TM_{0n}^a wave across the boundary.

R_n and T_n can be determined by satisfying the boundary condition at $\rho = a$. Using the analogy to wave propagation on a transmission line, we can address the boundary condition as the voltage from top to the bottom ground and the current on the bottom ground for each TM_{0n} mode are continuous at $\rho = a$. The condition can then be written as

$$\int_0^{d_t} E_{nz}^-|_{\rho=a}\,dz = \int_0^{d_t} E_{nz}^+|_{\rho=a}\,dz \tag{6a}$$

$$H_{n\phi}^-|_{\rho=a}^{z=0} = H_{n\phi}^+|_{\rho=a}^{z=0} \tag{6b}$$

where $d_t = d_1 + d_2 + d_3$, the total thickness of the MCA. E_{nz} and $H_{n\phi}$ are the z-directed electric intensity and ϕ-directed magnetic intensity of TM_{0n} mode. They can be evaluated from the magnetic potentials using $E_z = (\beta^2/j\omega\varepsilon)\Psi$ and $H_\phi = -(\partial\Psi/\partial\rho)$.

When using condition (6a), the following approximation is used to reduce the complexity:

$$\varepsilon_{r\mathrm{eff}} \equiv \left(\frac{\beta}{k_0}\right)^2 \approx \frac{d_t}{\displaystyle\int_0^{d_t} \frac{f(z)}{\varepsilon_r(z)}\,dz} \tag{7}$$

where $\varepsilon_{r\mathrm{eff}}$ is the effective relative dielectric constant of TM_0 in a radial waveguide. This approximation is reasonable when the conducting cover and ground plane of the MCA are close enough to each other that $k_{zi}d_i \ll 1$ with $k_{zi}^2 \equiv \varepsilon_{ri}k_0^2 - \beta_0^2$ and $i = 1$, 2, or 3. Using (6) and (7), we solve R_n and T_n as

$$R_n = \frac{T_n H_n^{(2)}(\beta_0^a a) - H_n^{(2)}(\beta_0^s a)}{H_n^{(1)}(\beta_0^s a)} \tag{8a}$$

$$R_{-n} = R_n, \qquad n = 0, 1, 2, \ldots \tag{8b}$$

and

$$T_n = \frac{H_n'^{(2)}(\beta_0^s a)\left[\dfrac{H_n^{(1)}(\beta_0^s a)}{H_n'^{(1)}(\beta_0^s a)} - \dfrac{H_n^{(2)}(\beta_0^s a)}{H_n'^{(2)}(\beta_0^s a)}\right]}{\beta_0^a H_n'^{(2)}(\beta_0^a a)\left[\dfrac{1}{\beta_0^s}\dfrac{H_n^{(1)}(\beta_0^s a)}{H_n'^{(1)}(\beta_0^s a)} - \dfrac{1}{\beta_0^a}\dfrac{H_n^{(2)}(\beta_0^a a)}{H_n'^{(2)}(\beta_0^a a)}\right]} \tag{9a}$$

$$T_{-n} = T_n, \qquad n = 0, 1, 2, \ldots. \tag{9b}$$

Using the Wronskian of Bessel's equation $J_n(x)N_n'(x) - N_nJ_n'(x) = 2/\pi x$, (9a) can be simplified to

$$T_n = \frac{4j}{\pi a}\Big/\Big[\beta_0^a H_n'^{(2)}(\beta_0^a a)H_n^{(1)}(\beta_0^s a) - \beta_0^s H_n'^{(1)}(\beta_0^s a)H_n^{(2)}(\beta_0^a a)\Big]. \tag{9c}$$

To finish evaluation of Ψ_c [see (5)], the coefficients a_n^c must be determined. These coefficients can be simply related to a set of coefficients a_n^b, which result when the radius of the sealant cover is extended to $\rho = \infty$ and radiation boundary condition assumed.

The magnetic potential of the TM_0^s waves in the four-layer structure can then be expressed as $\Psi_b = \sum_{n=-\infty}^{\infty} a_n^b H_n^{(2)}(\beta_0^s\rho)e^{jn\phi}f_s(z)$ where $\rho > \rho_0$. In region $\rho < a$, both Ψ_b and Ψ_c have the same dipole source. If we define a new field as $\Psi_d = \Psi_c - \Psi_b$, Ψ_d can be expressed as

$$\Psi_d = \sum_{n=-\infty}^{\infty}\Big((a_n^c - a_n^b)H_n^{(2)}(\beta_0^s\rho) + a_n^c R_n H_n^{(1)}(\beta_0^s\rho)\Big) \times e^{jn\phi}f_s(z), \qquad \rho_0 < \rho < a \tag{10}$$

and ψ_d is a source-free field in $\rho < a$. Therefore, the outward waves must be equal to the inward waves. This means the coefficients of $H_n^{(2)}(\beta_0^s\rho)$ and $H_n^{(1)}(\beta_0^s\rho)$ in (10) are equal, i.e., $a_n^c - a_n^b = a_n^c R_n$. The relation between a_n^c and a_n^b is then

$$a_n^c = \frac{a_n^b}{1 - R_n}. \tag{11}$$

If we define C_n as $a_n^b C_n = a_n^c T_n$, we can rewrite Ψ_c in the region of $\rho > a$ as

$$\Psi_c = \sum_{n=-\infty}^{\infty} a_n^b C_n H_n^{(2)}(\beta_0^a\rho)e^{jn\phi}f_a(z) \tag{12}$$

and express C_n as $C_n = T_n/(1 - R_n)$ from (11). Using the expressions of T_n and R_n in (8) and (9), we have (13), shown at the bottom of this page. C_n is a function of only β_0^s, β_0^a, and a. β_0^s and β_0^a are determined by the vertical layer structures with and without sealant layer and a is the radius of the sealant cover on a MMIC.

Using (4), (12), and the large argument approximation of Hankel function, the equivalent factor F can be written as

$$F = \frac{\displaystyle\sum_{n=-\infty}^{\infty} a_n^b C_n j^n e^{jn\phi}}{\displaystyle\sum_{n=-\infty}^{\infty} a_n^a j^n e^{jn\phi}}. \tag{14}$$

$$C_n = \frac{H_n^{(1)}(\beta_0^s a)}{\dfrac{\pi a}{2j}J_n(\beta_0^s a)\Big[\beta_0^s H_n'^{(1)}(\beta_0^s a)H_n^{(2)}(\beta_0^a a) - \beta_0^a H_n'^{(2)}(\beta_0^a a)H_n^{(1)}(\beta_0^s a)\Big] - H_n^{(2)}(\beta_0^a a)} \tag{13}$$

F is the function of ϕ and, thus, F is directional. Since the coupling system is reciprocal, we can also use F in (14) to determine the effective length of a receiving component. C_n can be calculated from (13). a_n^a and a_n^b can now be determined by solving for the TM_0 wave radiation of x-, y-, and z-dipoles in uniform multilayer structures of infinite lateral extent. This will be described in the Sections II-B and C.

B. Equivalent Factor For a z-Directed Dipole

By solving the TM_0 wave created by a unit z-directed dipole of length d_1 in layer 1 at (ρ_0, ϕ_0), we obtain (see Appendix B)

$$\Psi_a = \frac{-\omega\varepsilon_{r1}\beta_0^a}{2(k_{z1}^a)^3 d_1 \sin(k_{z1}^a d_1)} \mathrm{Res}\left[Q_{\mathrm{TM}}^a(\beta_0^a)\right] \times H_0^{(2)}(\beta_0^a|\vec{\varrho}-\vec{\varrho}_0|)\cos(k_{z1}^a z) \tag{15a}$$

$$\Psi_b = \frac{-\omega\varepsilon_{r1}\beta_0^s}{2(k_{z1}^s)^3 d_1 \sin(k_{z1}^s d_1)} \mathrm{Res}\left[Q_{\mathrm{TM}}^s(\beta_0^s)\right] \times H_0^{(2)}(\beta_0^s|\vec{\varrho}-\vec{\varrho}_0|)\cos(k_{z1}^s z), \qquad 0<z<d_1. \tag{15b}$$

k_{z1}^i is defined as $(k_{z1}^i)^2 = \varepsilon_{r1}k_0^2 - (\beta_0^i)^2$, where i stands for a or s. Q_{TM}^i is a function of β (see Appendix A), which contains the information about the layered structure. It has a pole at $\beta=\beta_0^i$ with an associated residue, $\mathrm{Res}[Q_{\mathrm{TM}}^i(\beta_0^i)]$.

Applying the *addition theorem* [6] to the Hankel function in (15a) and comparing the resulting expression to (4) results in an expression for a_n^a as follows:

$$a_n^a = \frac{-\omega\varepsilon_{r1}\beta_0^a}{2(k_{z1}^a)^3 d_1 \sin(k_{z1}^a d_1)} \mathrm{Res}\left[Q_{\mathrm{TM}}^a(\beta_0^a)\right] J_n(\beta_0^a\rho_0)e^{-jn\phi_0}, \qquad -\infty<n<\infty. \tag{16a}$$

In the same way, we obtain

$$a_n^b = \frac{-\omega\varepsilon_{r1}\beta_0^s}{2(k_{z1}^s)^3 d_1 \sin(k_{z1}^s d_1)} \mathrm{Res}\left[Q_{\mathrm{TM}}^s(\beta_0^s)\right] \times J_n(\beta_0^s\rho_0)e^{-jn\phi_0}, \qquad -\infty<n<\infty. \tag{16b}$$

From (14) and (16), we obtain the equivalent factor of the z-directed dipole

$$F_z = \frac{\beta_0^s \mathrm{Res}\left[Q_{\mathrm{TM}}^s(\beta_0^s)\right](k_{z1}^a)^3 \sin(k_{z1}^a d_1)}{\beta_0^a \mathrm{Res}\left[Q_{\mathrm{TM}}^a(\beta_0^a)\right](k_{z1}^s)^3 \sin(k_{z1}^s d_1)} \times \frac{C_0 J_0(\beta_0^s\rho_0) + 2\sum_{n=1}^{\infty} C_n j^n J_n(\beta_0^s\rho_0)\cos\left(n(\phi-\phi_0)\right)}{J_0(\beta_0^a\rho_0) + 2\sum_{n=1}^{\infty} j^n J_n(\beta_0^a\rho_0)\cos\left(n(\phi-\phi_0)\right)}. \tag{17}$$

As we can see, the first term on the right-hand side of (17) only depends on the layer structure, but the second term is the function of ρ_0 and $(\phi-\phi_0)$. Therefore, F_z varies with the location of the source dipole and the angle to the field point.

In (17), two infinite summations need to be evaluated. In the MCA, we are currently considering, the transverse extent of the MMIC is small relative to a TM_0 parallel-plate wavelength, i.e., $\beta_0\rho_{0\ \max}$ is small. $2\rho_{0\ \max}$ is the largest dimension of the MMIC. If $|\beta_0\rho_{0\ \max}|<1$, $J_n(\beta_0\rho_{0\ \max})$ drops very quickly to zero as n increases. Therefore, the two summations can be accurately evaluated by summing only the first several items, e.g., $N_{\max}=3$.

C. Equivalent Factor for a Surface Current Dipole

Any surface current on the surface of the substrate under the sealant cover can be decomposed into the two respective components I_xL_x and I_yL_y. To determine an equivalent-surface current dipole, we need to find the equivalent factors F_x and F_y.

As was done in the previous section, we first obtain the TM_0 wave created by a unit x-directed dipole at (ρ_0, ϕ_0) on the surface of the bottom layer as follows:

$$\Psi_a = \frac{-\omega\varepsilon_{r1}}{2\beta_0^a k_{z1}^a \sin(k_{z1}^a d_1)} \mathrm{Res}\left[Q_{\mathrm{TM}}^a(\beta_0^a)\right] \times \frac{\partial}{\partial x}\left[H_0^{(2)}(\beta_0^a|\vec{\rho}-\vec{\rho}_0|)\right]\cos(k_{z1}^a z) \tag{18a}$$

$$\Psi_b = \frac{-\omega\varepsilon_{r1}}{2\beta_0^s k_{z1}^s \sin(k_{z1}^s d_1)} \mathrm{Res}\left[Q_{\mathrm{TM}}^s(\beta_0^s)\right]\frac{\partial}{\partial x} \times \frac{\partial}{\partial x}\left[H_0^{(2)}(\beta_0^s|\vec{\rho}-\vec{\rho}_0|)\right]\cos(k_{z1}^s z), \qquad 0<z<d_1. \tag{18b}$$

Then use the *addition theorem* to put (18) into the form of (4). We obtain

$$a_n^a = \frac{-\omega\varepsilon_{r1}}{2\beta_0^a k_{z1}^a \sin(k_{z1}^a d_1)} \mathrm{Res}\left[Q_{\mathrm{TM}}^a(\beta_0^a)\right] \times \left[J_{n+1}(\beta_0^a\rho_0)e^{j(\phi-\phi_0)} - J_{n-1}(\beta_0^a\rho_0)e^{-j(\phi-\phi_0)}\right] \times \frac{e^{-jn\phi_0}}{\cos\phi}, \qquad -\infty<n<\infty \tag{19a}$$

and

$$a_n^b = \frac{-\omega\varepsilon_{r1}}{2\beta_0^s k_{z1}^s \sin(k_{z1}^s d_1)} \mathrm{Res}\left[Q_{\mathrm{TM}}^s(\beta_0^s)\right] \times \left[J_{n+1}(\beta_0^s\rho_0)e^{j(\phi-\phi_0)} - J_{n-1}(\beta_0^s\rho_0)e^{-j(\phi-\phi_0)}\right] \times \frac{e^{-jn\phi_0}}{\cos\phi}, \qquad -\infty<n<\infty. \tag{19b}$$

From (14) and (19), we obtain the equivalent factor for an x-directed dipole [see (20) at the bottom of the following page.]

In the same way, we can solve F_y. It turns out $F_y = F_x$. Therefore, we can define an equivalent factor of any surface current dipole as F_ρ and

$$F_\rho \equiv F_y = F_x. \tag{21}$$

Expressions (20) and (21) show that F_ρ and F_z have similar characteristics. First, F_ρ varies with the location of the surface current dipole and the angle to the field point. Second, the two semi-infinite summations can be accurately evaluated using only the first several terms, when $|\beta_0\rho_{0\ \max}|<1$.

III. The Algorithm

Fig. 3 overviews the entire algorithm we propose for the coupling between dielectric block-covered MMICs. This algorithm is developed for use in conjunction with a layout-based circuit

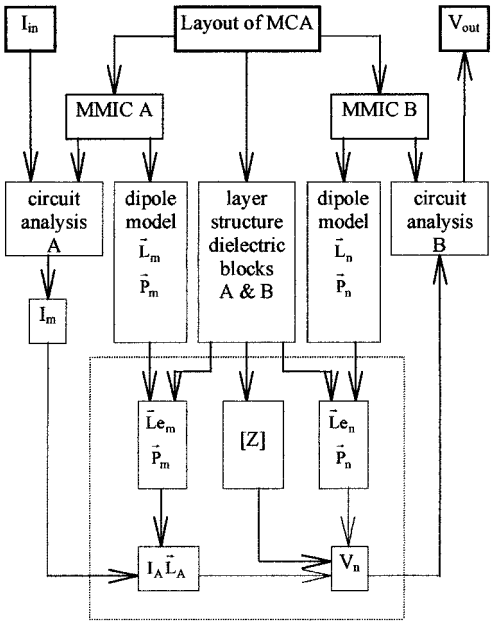

Fig. 3. Flow diagram of the algorithm

CAD software. We apply it on the HP EEsof Microwave Design System (MDS).[1]

The algorithm starts from the layout of the MCA assuming, e.g., two MMICs. First, the schematics of MMIC A and B are extracted from the layout. We excite the ports of MMIC A using the circuit simulation and obtain the input currents I_m for each of its components (spiral inductors, MIM capacitors, stubs, etc.).

An equivalent length is associated with every component and stored in the simulator component library. The necessary library expressions can be determined analytically for most components. In Fig. 3, $\vec{L}_m$ and $\vec{L}_n$ represent the equivalent lengths of component m in MMIC A and component n in MMIC B, and $\vec{P}_m$ and $\vec{P}_n$ represent the locations of the components. The layer structure of the MCA and dielectric blocks on MMIC A and B are also known. The equivalent uncovered dipole lengths $\vec{L}e_m$ and $\vec{L}e_n$ are then evaluated with the simplification technique described in the previous section.

By summing $I_m\vec{L}e_m$ over all m, the x-, y-, and z-directed macrodipoles (I_xL_x, I_yL_y, and I_zL_z) representing MMIC A are determined. Using $\vec{P}_m$ and the procedure in [1], we determine $\vec{P}_x$, $\vec{P}_y$, and $\vec{P}_z$, the locations of the macrodipoles. As described in [1], we calculate the induced voltage V_n on the nth component of MMIC B by

$$V_n = \vec{L}e_n \cdot [Z] \cdot I_A\vec{L}_A \tag{22}$$

where $I_A\vec{L}_A = [I_xL_x,\, I_yL_y,\, I_zL_z]^T$ is the macrodipole set representing MMIC A, and $\vec{L}e_n$ is the equivalent length of the n'th component in MMIC B. $[Z]$ is an analytical expression that depends on the layered structure of the MCA outside the sealant covers, the macrodipole locations, and the field points in MMIC B. (see [1, Appendix A]).

The last step is to plug the voltage sources V_n into MMIC B's circuit model and then use the circuit simulator to get the voltages at the output ports of MMIC B. Further processing can easily calculate the S-parameters that described the coupling between a port on MMIC A and one on MMIC B.

In Fig. 3, all the procedures outside the dotted-line frame are done with the aid of the MDS circuit simulator. An external program does the calculation inside the frame. Note that the approximate current distribution on the MMIC surface is found by the circuit simulator and not by using a full electromagnetic (EM) analysis.

When we apply this algorithm in a CAD tool, the following are a few practical problems that need to be considered.

- We assume the sealant cover is circular. However, as we mentioned before, the real cover may be shaped like a square with round corners or some other quasi-circular shape. Therefore, we have to find a satisfactory circular cover to represent the real one. We choose this circle to be the average of the largest circumcircle and smallest inscribed circle, i.e., it is centered right between the centers of these two circles and has the average radius of these two radii.
- As we discussed previously, an equivalent factor F (F_z or F_ρ) for a dipole in MMIC A varies with the angle to the location of each component of MMIC B. If the sealant covers on MMIC A and B are centered at $\vec{\rho}_{cA}$ and $\vec{\rho}_{cB}$ with radii of r_A and r_B, respectively, these angles are within the range of $\phi_{cB} \pm \phi_{\max B}$, where $\phi_{cB} = \angle(\vec{\rho}_{cB} - \vec{\rho}_{cA})$ and $\phi_{\max B} = \sin^{-1}(r_B/|\vec{\rho}_{cB} - \vec{\rho}_{cA}|)$. $\phi_{\max B}$ is usually small since we assume MMIC A and B are widely separated and their size are relatively small. If $\phi_{\max B}$ is small enough, i.e., $\phi_{\max B} < 10°$, we can approximate the detail angle ϕ as ϕ_{cB} in both (17) and (20) when determining the equivalent factor for block-covered dipole in MMIC A. This approximation will greatly reduce the

[1]Hewlett-Packard Company, Santa Rosa, CA.

$$F_x = \frac{\mathrm{Res}\left[Q^s_{\mathrm{TM}}(\beta^s_0)\right] k^a_{z1}\, \sin(k^a_{z1}d_1)}{\mathrm{Res}\left[Q^a_{\mathrm{TM}}(\beta^a_0)\right] k^s_{z1}\, \sin(k^s_{z1}d_1)} \times \frac{C_0 J_1(\beta^s_0\rho_0)\cos(\phi-\phi_0)+}{J_1(\beta^a_0\rho_0)\cos(\phi-\phi_0)+} \cdots$$
$$\cdots \frac{\displaystyle\sum_{n=1}^{\infty} C_n j^n \Big[J_{n+1}(\beta^s_0\rho_0)\cos\big((n+1)(\phi-\phi_0)\big) - J_{n-1}(\beta^s_0\rho_0)\cos\big((n-1)(\phi-\phi_0)\big)\Big]}{\displaystyle\sum_{n=1}^{\infty} j^n \Big[J_{n+1}(\beta^a_0\rho_0)\cos\big((n+1)(\phi-\phi_0)\big) - J_{n-1}(\beta^a_0\rho_0)\cos\big((n-1)(\phi-\phi_0)\big)\Big]}. \tag{20}$$

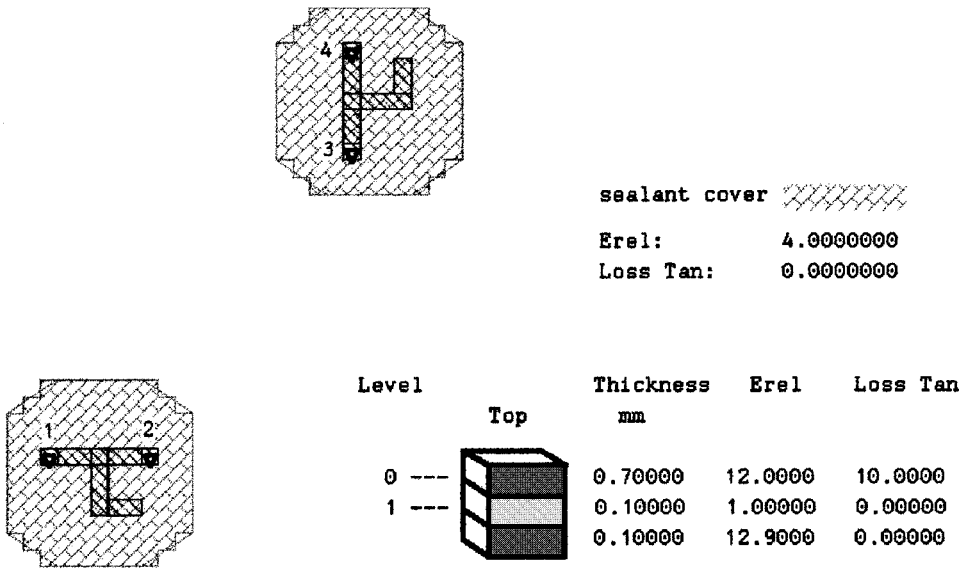

Fig. 4. ***em*** set up for analysis of coupling between two-port stub/thru-line circuit under dielectric block covers.

calculation time without sacrificing too much accuracy. When evaluating the equivalent factor for a block-covered receiving component in MMIC B, similar approximation can be made, i.e., replacing the angle to the dipole with the angle to the center of MMIC A.

IV. Comparison to Numerical Simulation—Anechoic Enclosure

In order to assess the accuracy of this algorithm, we have compared the result of our algorithm to the one obtained from a full-wave analysis using Sonnet Software's ***em***,[2] a method-of-moments simulator. Sonnet's Dielectric Bricks capability allows structures with dielectric inhomogeneities to be analyzed. We utilize this feature to simulate the coupling between two very simple test circuits with dielectric covers. However, it is very CPU time and memory intensive.

We have chosen two two-port microstrip stub circuits for our verification tests. Fig. 4 shows the configuration of these two circuits in the ***em*** simulator. Each circuit consists of a stub in shunt with a through line that has a via connection on each end to ports in the ground plane. All microstrips are 0.2-mm wide. The circuits are each covered by a chamfered square dielectric block with $\varepsilon_r = 4$ and the same thickness as the middle layer of the three package layers. All other dimensions can be inferred from this figure. In this test case, the loss tangent of the top layer is chosen to be ten so that the parallel-plate wave launched by the circuits is damped to a negligible level by the time it reflects from one of the simulator's sidewalls. Hence, we do not have to consider resonances or other wall effects.

Fig. 5 compares $|S_{42}|$ computed using our algorithm to the ***em*** simulation of the same structure. The difference between the two results is less than 1.5 dB in the -50 to -60-dB range. The third curve in the figure is the ***em*** simulation result for the same two circuits without dielectric covers. It shows that the dielectric covers have a significant effect on the coupling between the two

[2]***em*** is a trademark of SONNET Inc., Liverpool, NY.

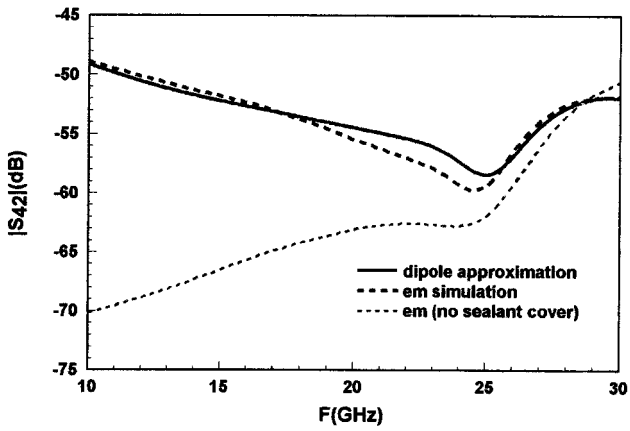

Fig. 5. S-parameter magnitude of the coupling between ports 2 and 4 of the circuit illustrated in Fig. 4. The dashed thin line shows coupling without dielectric covers.

circuits—increasing the coupling by 20 dB at low frequencies. Our algorithm correctly predicts this increase.

Our algorithm used in conjunction with MDS simulates 200 frequency points between 10–30 GHz in 10 s. Sonnet's ***em*** requires about 7 h to finish 40 frequency points simulation. In this example, the algorithm uses three orders of magnitude less time than the full-wave EM simulator.

V. Modified Algorithm for Finite-Size Enclosures

A similar approach is developed for an enclosure with perfectly conducting sidewalls by using the method of images. In this procedure, the MCA bounded by perfectly conducting walls is replaced by an MCA of infinite lateral extent plus an infinite set of image sources [1], [5]. The field at a particular point can then be determined by summing the fields contributed by each member of this set—an infinite set of dielectric covered dipoles. This approach allows the analysis developed in the preceding sections to be used in a straightforward manner. In MCAs that

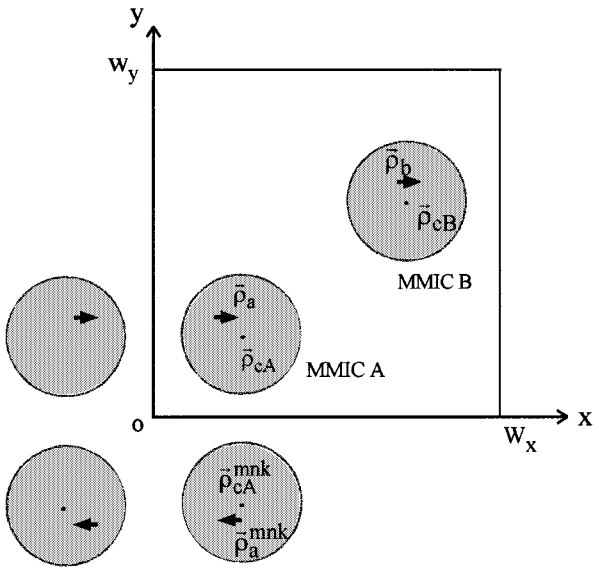

Fig. 6. Schematic drawing of an enclosed dielectric block-covered dipole in MMIC A and a few of the infinite set of image dielectric block-covered dipoles.

have a damping layer, the number of images necessary can be truncated to a reasonable level. If necessary, the double summation of images fields can be converted to a very computationally efficient form [5].

When radiating currents are covered with blocks of dielectric, each image current must be also be covered with dielectric. The infinitely extended MCA consists of an infinite set of dielectric blocks, each covering several radiating dipoles. To simplify the analysis of such a structure, each block-covered dipole is replaced by an equivalent uncovered dipole as determined by the process described in earlier sections. Normally a wave excited from a dipole would scatter from a number of dielectric blocks as it travels through the extended MCA. Since in our algorithm all the block-covered dipoles are replaced by uncovered dipoles, we have neglected this scattering.

To show how the image technique is applied, consider a radiating dipole I_aL_a at $\vec{\rho}_a$ and a receiving component with effective length L_b at $\vec{\rho}_b$ in Fig. 6. Each of them is covered by a circular dielectric block centered at $\vec{\rho}_{cA}$ and $\vec{\rho}_{cB}$, respectively. Using method of images, we first create an infinite set of dipoles located at $\vec{\rho}_a^{mnk}$ and covered by sealant covers centered at $\vec{\rho}_{cA}^{mnk}$ in an infinite extended MCA. If we present $\vec{\rho}_a$ and $\vec{\rho}_{cA}$ as (x_a, y_a) and (x_{cA}, y_{cA}), respectively, $\vec{\rho}_a^{mnk}$ and $\vec{\rho}_{cA}^{mnk}$ can be expressed as

$$\begin{aligned}
\vec{\rho}_a^{mn0} &= (2mw_x + x_a,\, 2nw_y + y_a)\\
\vec{\rho}_{cA}^{mn0} &= (2mw_x + x_{cA},\, 2nw_y + y_{cA})\\
\vec{\rho}_a^{mn1} &= (2mw_x + x_a,\, 2nw_y - y_a)\\
\vec{\rho}_{cA}^{mn1} &= (2mw_x + x_{cA},\, 2nw_y - y_{cA})\\
\vec{\rho}_a^{mn2} &= (2mw_x - x_a,\, 2nw_y + y_a)\\
\vec{\rho}_{cA}^{mn2} &= (2mw_x - x_{cA},\, 2nw_y + y_{cA})\\
\vec{\rho}_a^{mn3} &= (2mw_x - x_a,\, 2nw_y - y_a)\\
\vec{\rho}_{cA}^{mn3} &= (2mw_x - x_{cA},\, 2nw_y - y_{cA})
\end{aligned}$$

and

$$k = 0,\, 1,\, 2,\, 3. \tag{23}$$

The effect of the complete set of images is achieved by calculating the induced voltage on receiving component b that results from summing the contributions from dipoles with location indexes m, n over the range $-\infty < m,\, n < \infty$ and k over the range $k = 0,\, 1,\, 2,\, 3$. This can be done by following the procedure described in Section III.

In the procedure, the equivalent factor F_a^{mnk} for each dielectric block-covered dipole in MMIC A will be evaluated using (17) or (20). The parameters ρ_0, ϕ_0, and ϕ used in the equations for F_a^{mnk} are

$$\begin{aligned}
\rho_0 &= \left|\vec{\rho}_a^{mnk} - \vec{\rho}_{cA}^{mnk}\right| = \left|\vec{\rho}_a - \vec{\rho}_{cA}\right|\\
\phi_0 &= \angle\left(\vec{\rho}_a^{mnk} - \vec{\rho}_{cA}^{mnk}\right) = \angle\left(\vec{\rho}_a - \vec{\rho}_{cA}\right)\\
\phi &= \angle\left(\vec{\rho}_{cB} - \vec{\rho}_{cA}^{mnk}\right).
\end{aligned} \tag{24}$$

In (24), $\vec{\rho}_{cB}$ is used to replace $\vec{\rho}_b$ when determining ϕ. The reason for this approximation is explained in Section III. Equation (24) shows that the angle $\phi - \phi_0$ can be any value between $-180°$–$180°$. However, since $\phi - \phi_0$ is used with a cosine function in (17) and (20), the factor only must be evaluated between 0°-180°. Also, in practice, it is only necessary to evaluate the factor once for any fixed interval $\Delta\varphi$, e.g. 15°. If we choose $\Delta\varphi$ to be 15°, only 12 equivalent factors are need to fully evaluate the a set of equivalent factors for the dielectric block-covered dipole a and its images.

A set of equivalent factors is also needed for each component in MMIC B, one factor for each radiating dipole and one for each of its images. The parameters ρ_0, $\phi_0$and ϕ used in the (17) or (20) for F_b^{mnk} are then

$$\begin{aligned}
\rho_0 &= \left|\vec{\rho}_b - \vec{\rho}_{cB}\right|\\
\phi_0 &= \angle\left(\vec{\rho}_b - \vec{\rho}_{cB}\right)\\
\phi &= \angle\left(\vec{\rho}_{cA}^{mnk} - \vec{\rho}_{cB}\right).
\end{aligned} \tag{25}$$

Once these equivalent factors are evaluated, the induced voltage source on receiving component b due to each dipole can be calculated. Summing all the voltage sources together, we obtain the total induced voltage source on component b due to the radiating dipoles a in the bounded MCA. If both the radiating dipole a and receiving component b are x-directed, the expression for the induced voltage source V_{ba} is

$$V_{ba} = \sum_{n=-\infty}^{\infty}\sum_{m=-\infty}^{\infty}\sum_{k=0}^{3} F_b^{mnk} L_b Z_{xx}\left(\left|\vec{\rho}_b - \vec{\rho}_a^{mnk}\right|\right) \cdot I_a L_a F_a^{mnk} SX(k) \tag{26}$$

where Z_{xx} is one of the elements in $[Z]$ and $SX(k)$ takes on values $SX = [1, -1, 1, -1]$. The value of $SX(k)$ depends on whether the particular image dipole is in the same, or opposite, direction as the primary dipole. For a y-directed primary dipole, Z_{xx} and SX are replaced by Z_{xy} and $SY = [1, 1, -1, -1]$, respectively. For a z-directed primary dipole, Z_{xx} and SX are replaced by Z_{xz} and $SZ = [1, -1, -1, 1]$, respectively.

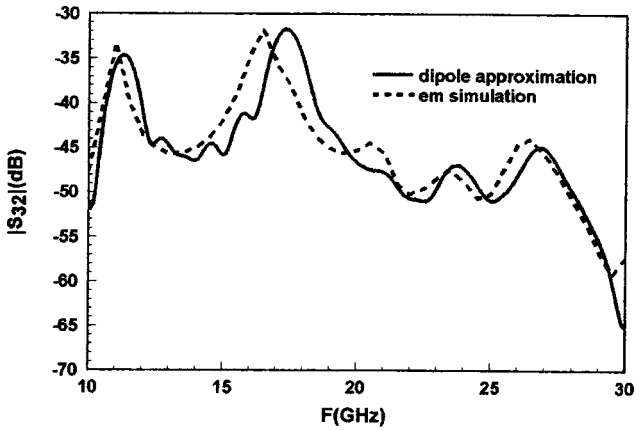

Fig. 7. Coupling between two sealant covered two-port circuits in an 8 mm × 8 mm box with a damping layer having a loss tangent of 0.1.

VI. Comparison to Numerical Simulation—Finite-Size Enclosure

Coupling between two test circuits with sealant covers in a moderate Q enclosure is computed using the full-wave analysis package ***em*** with Sonnet's Dielectric Bricks feature and using the modified algorithm described above. The loss tangent of the damping layer is 0.1. The box size is 8 × 8 mm. The two circuits are identically the same as the one in Fig. 4 with two ports marked 1 and 2, except that the thickness of the sealant cover is only half of the thickness of the middle layer. The centers of each sealant cover are separated from each other by 5 mm. Fig. 7 shows $|S_{32}|$ determined from a full-wave simulation and from our modified dipole approximation algorithm. Note the greatly increased coupling that occurs at the resonance frequencies introduced by the box. The result shows the good agreement between the two methods. However, the resonance frequencies predicted by the two methods are a little different. This is because we neglect the effect of the sealant cover on the box resonance in our algorithm. A wave travels slower through the region with a dielectric block than in other areas. Since we neglect the existence of the sealant islands on the path of TM_0 wave travel, the resonant frequencies predicted by our algorithm is slightly higher. As long as the permittivity of dielectric block is low and/or its thickness is much thinner than the free-space layer, the resonant frequency will not change significantly.

The total calculation time of our algorithm with the aid of MDS is about a couple of minutes, which is at least two orders of magnitude faster than ***em*** run on an HP-715 workstation.

VII. Conclusion

An algorithm has been described for computing the coupling between dielectric-covered MMICs in a multichip module. This algorithm is modified by comparison to the algorithm in [1] by including the effect that the dielectric cover has on the radiation of the MMIC. The assumption used in modifying the algorithm in [1] are that: 1) the sealant cover is shaped like a circular or quasi-circular and 2) the sealant cover is thin.

We have verified the algorithm by comparing its predictions to those of a numerically rigorous method-of-moments simulations for several test cases. The new algorithm uses orders of magnitude less CPU time than the rigorous simulator for these test circuits. For typically sized MMICs, with hundreds of components in each MMIC, a full method-of-moments simulation would be impractical, and approximate calculations such as we describe are the only reasonable alternative. Applying the technique to such an application will have to await the development of an interface to layout-based CAD.

Appendix A
Q^a_{TM} and Q^s_{TM} Formula

$$Q^a_{\mathrm{TM}} = \frac{1}{Y_L^{(1)} + Y_R^a} \tag{A1}$$

$$Y_L^{(1)} = -jY_{\mathrm{TM}}^{(1)} \cot(k_{z1}d_1) \tag{A2}$$

$$Y_R^{(3)} = -jY_{\mathrm{TM}}^{(3)} \cot(k_{z3}d_3) \tag{A3}$$

$$Y_R^a = Y_{\mathrm{TM}}^{(2)} \frac{Y_R^{(3)} + jY_{\mathrm{TM}}^{(2)} \tan(k_{z2}d_2)}{Y_{\mathrm{TM}}^{(2)} + jY_R^{(3)} \tan(k_{z2}d_2)} \tag{A4}$$

$$Y_{\mathrm{TM}}^{(i)} = \frac{\varepsilon_{ri}k_0}{k_{zi}\eta_0}, \qquad i = 1, 2, 3$$

$$k_{zi}^2 = \varepsilon_{ri}k_0^2 - \beta_0^2$$

$$Q^s_{\mathrm{TM}} = \frac{1}{Y_L^{(1)} + Y_R^s} \tag{A5}$$

$$Y_R^{(a)} = Y_{\mathrm{TM}}^{(2)} \frac{Y_R^{(3)} + jY_{\mathrm{TM}}^{(2)} \tan\left(k_{z2}(d_2 - d_s)\right)}{Y_{\mathrm{TM}}^{(2)} + jY_R^{(3)} \tan\left(k_{z2}(d_2 - d_s)\right)} \tag{A6}$$

$$Y_R^{(s)} = Y_{\mathrm{TM}}^{(s)} \frac{Y_R^{(a)} + jY_{\mathrm{TM}}^{(s)} \tan(k_{zs}d_s)}{Y_{\mathrm{TM}}^{(s)} + jY_R^{(a)} \tan(k_{zs}d_s)} \tag{A7}$$

$$Y_{\mathrm{TM}}^{(s)} = \frac{\varepsilon_{rs}k_0}{k_{zs}\eta_0}, \qquad k_{zs}^2 = \varepsilon_{rs}k_0^2 - \beta_0^2.$$

Appendix B
Derivation of Equations (15) and (18)

Starting from [1, eqs. (A5) and (A9)]

$$Z_{zx} = \frac{-j\beta_0}{2k_{z1}^2 d_1^2} \operatorname{Res}\left[Q_{\mathrm{TM}}(\beta_0)\right] \frac{\partial}{\partial x} H_0^{(2)}\left(\beta_0|\vec{\varrho} - \vec{\varrho}_0|\right) \tag{B1}$$

$$Z_{zz} = \frac{-j\beta_0^3}{2k_{z1}^4 d_1^2} \operatorname{Res}\left[Q_{\mathrm{TM}}(\beta_0)\right] H_0^{(2)}\left(\beta_0|\vec{\varrho} - \vec{\varrho}_0|\right) \tag{B2}$$

where

$$Z_{zj} \equiv \frac{-1}{d_1} \left[\int_0^{d_1} dz\, E_z(\rho, z)\right] \Big/ LI \tag{B3}$$

and j can be either x or z. (In [1] two typographical errors were made: 1) an additional d_1 should appear in the denominator of [1, eqs. (A5) and (A6)] and 2) the d_1 in the denominator of (B3) above was omitted.) In the following, we assume a unit strength electric dipole ($LI = 1$).

Since $E_z = (\beta^2/j\omega\varepsilon)\Psi$ and since we know that $\Psi \propto \cos(k_{z1}z)$ for $0 < z < d_1$, then

$$Z_{zj} \equiv \frac{-\beta_o^2}{j\omega\varepsilon_1 d_1}\left[\int_0^{d_1} dz\Psi(\rho, z)\right] = \frac{-\beta_o^2}{j\omega\varepsilon_1 d_1}\frac{\Psi(\rho, z)}{\cos(k_{z1}z)}\frac{\sin(k_{z1}d_1)}{k_{z1}}. \quad \text{(B4)}$$

Rearranging (B4) results in

$$\Psi(\rho, z) = \frac{-j\omega\varepsilon_1 k_{z1} d_1}{\beta_o^2 \sin(k_{z1}d_1)} Z_{zj} \cos(k_{z1}z). \quad \text{(B5)}$$

When $j = z$, and (B2) is inserted in (B5), (15) results. When $j = x$, and (B1) is inserted in (B5), (18) results.

REFERENCES

[1] R. W. Jackson and Z. Wang, "Circuit model for coupling between MMIC's in multichip modules including resonance effects," *IEEE Trans. Microwave Theory Tech.*, vol. 46, pp. 959–965, July 1998.

[2] X. Cai, K. Nabors, and J. White, "Efficient Galerkin techniques for multipole-accelerated capacitance extraction of 3-D structures with multiple dielectrics," in *Proc. Advanced Res. VLSI Conf.*, Chapel Hill, NC, 1995, pp. 200–211.

[3] S. M. Rao and T. K. Sarkar, "Static analysis of arbitrarily shaped conducting and dielectric structures," *IEEE Trans. Microwave Theory Tech.*, vol. 46, pp. 1171–1173, Aug. 1998.

[4] Z. Wang and R. W. Jackson, "A CAD algorithm for coupling between dielectric covered MMIC's in multi-chip assemblies," in *IEEE Int. MTT-S Microwave Symp. Dig.*, June 1998, pp. 33–36.

[5] R. W. Jackson, "The use of sidewall images to compute package effects in MoM analysis of MMIC circuits," *IEEE Trans. Microwave Theory Tech.*, vol. 41, pp. 406–414, Mar. 1993.

[6] R. F. Harrington, *Time Harmonic Electromagnetics Fields*. New York: McGraw-Hill, 1961.

Zhaoyang Wang (S'98) was born in Shanghai, China, in 1971. He received the B.S. degree in electrical engineering from the University of Science and Technology of China, Hefei, China, in 1993, and is currently working toward the Ph.D. degree at the University of Massachusetts at Amherst.

From 1994 to 1996, he was a Research Assistant in the Laboratory for Millimeter Wave Devices and Applications, Department of Electrical and Computer Engineering, University of Massachusetts at Amherst. Since 1997, he has been involved with circuit modeling of packaged MMICs in the Laboratory for Millimeter Waves and Space Applications. His research interests have included the investigation and characterization of solid-state detectors in the terahertz frequency range, focusing on superconducting hot electron bolometer (HEB) receivers. His research interests also include MMIC integrated circuit (IC) design and RF CMOS circuit design.

Robert W. Jackson (M'82–SM'88) received the B.S., M.S., and Ph.D. degrees from Northeastern University, Boston, MA, in 1975, 1979, and 1981, respectively.

From 1981 to 1982, he was an Assistant Professor in the Department of Electrical Engineering, Northeastern University. In 1982, he joined the University of Massachusetts at Amherst, where he is currently an Associate Professor. His primary research and teaching interests center on MW and MMW electronics, especially ICs. In particular, he has contributed in the areas of numerical modeling of microstrip and coplanar-waveguide circuits, novel printed structures in coplanar waveguide, and the modeling of packages for MW and MMW ICs. He has also developed CAD routines for ferrite phase-shifter design and consulted on topics connected with fiber optics for MW applications.